A Linear Complementarity based MPC for Aerial Physical Interaction

Riccardo Fuser, Hai-Nguyen Nguyen, Gian Paolo Incremona, Marcello Farina, Marco Cognetti

A Linear Complementarity based MPC for Aerial Physical Interaction

Riccardo Fuser[1], Hai-Nguyen Nguyen[2], Gian Paolo Incremona[3], Marcello Farina[3], Marco Cognetti[1]

***Abstract*— This paper presents a general MPC-based control framework that includes the linear complementarity problem (LCP) for modeling the interaction forces of a mobile robot. To validate our approach, two case studies are considered: (i) an aerial robot that should reach a target point placed on a frictionless surface; and (ii) an aerial robot that should lift a cable-suspended mass, switching from a slack to a taut cable condition. The simulation results confirm the validity of our approach, and the ability of the LCP to model the interaction forces for an aerial platform.**

I. Introduction

In recent years, aerial robotics has experienced an extreme growth in popularity also thanks to the rapid evolution of technology [1], [2]. Aerial robots have found application in a wide range of civilian and commercial uses, stemming from aerial photography and cinematography [3] to aerial monitoring and inspections [4]. All these activities involve purely observations of the environment. This contrasts with one of the goals of robotics, which includes developing autonomous systems capable of assisting and/or replacing humans in demanding or hazardous tasks [5], especially in hard-to-reach environments like high altitudes, or areas with radiation exposure. To achieve this goal, aerial robots must not only observe their surroundings but also actively interact with them, managing the interaction forces that arise.

Along this line, research is now focusing on the development of aerial manipulators – that is, aerial platforms equipped with robotic arms – explicitly meant for active interaction with the environment [1]. These systems can be employed in a variety of applications, including contact-based inspection [6], industrial maintenance [7], and disaster response [8]. Beyond manipulation, another emerging form of physical interaction for aerial platforms involves payload transportation, where the robot must exchange forces with the payload to move it toward a desired location [9]. In this context, [10], [11] propose the use of multiple Autonomous Aerial Vehicles (AAVs) connected to the payload via cables to enable cooperative aerial transportation.

The possibility to interact with the environment can be useful also for energy-saving purposes, in order to overcome the limitation of the aerial robots' short endurance. For example, AAVs encaged in external protective structures, typically spherical or cylindrical, have been developed in [12], [13]. When the external protecting cage is a rolling structure, a hybrid design is obtained which makes it possible for both aerial and terrestrial locomotion and, at the same time, it gives the possibility to limit energy consumption by making use of the terrestrial locomotion whenever practicable.

These recent developments in aerial physical interaction highlight the increasing complexity of tasks involving direct contact with the environment. An important challenge in such scenarios lies in accurately modeling the interaction itself. Even more critically, an open question is how to represent the transition between contact and non-contact phases, which is essential for ensuring stable and reliable behavior during dynamic interactions. Motivated by these considerations, we use a Linear Complementarity Problem (LCP) [14], [15] to model the physical interaction. The latter can be integrated inside a Model Predictive Controller (MPC) [16]–[18]. The MPC is efficiently solved by the iterative Linear Quadratic Regulator (iLQR) algorithm [15], [19], [20].

In this paper, the effectiveness of the proposed framework is demonstrated on two case studies: (i) a quadrotor that should land on a frictionless surface, and (ii) a quadrotor that must lift a cable-suspended payload. It is worth highlighting that modeling the interaction through a LCP formulation enables the derivation of a unified model, eliminating the need to separately model the pre- and post-contact phases and to design a hybrid control strategy to handle the switching between them. This is particularly advantageous in the second scenario, which is typically represented in the literature as a hybrid system composed of multiple discrete modes. For instance, in [21], the lifting maneuver is segmented into three distinct phases – setup, pull, and raise – each governed by its own set of dynamics. In contrast, our approach employs a single, continuous model, which is more naturally suited for integration within an MPC framework.

The rest of the paper is organized as follows. Section II presents the LCP-based models developed for the considered case studies. Section III formulates the MPC problem and outlines its application to the different scenarios. Simulation results validating the proposed approach are reported in Section IV. Finally, Section V concludes the paper.

II. Modeling

This section derives the LCP formulation to model interaction forces acting on a robot. In particular, Section II-A describes some preliminaries, Section II-B derives its mathematical formulation, while Section II-C presents the

[1]R. Fuser and M. Cognetti are with the LAAS-CNRS, Université de Toulouse, CNRS, Toulouse, France. email: {riccardo.fuser, marco.cognetti}@laas.fr

[2]H. Nguyen is with the RMIT University Vietnam, Saigon South Campus, Vietnam. email: hainguyen.nguyen@rmit.edu.vn

[3]G. P. Incremona and M. Farina is with the Dipartimento di Elettronica, Informazione e Bioingegneria, Politecnico di Milano, 20133 Milan, Italy. email: {gianpaolo.incremona, marcello.farina}@polimi.it

This work was supported by the Chaire de Professeur Junior Grant ANR-22-CPJ1-0064-01 and by the Italian Ministry of Enterprises and Made in Italy in the framework of the project 4DDS (4D Drone Swarms) under grant no. F/310097/01-04/X56.

two case studies considered in this paper: (i) a planar quadrotor that should land on a frictionless surface, and (ii) a planar quadrotor that should lift a cable-suspended payload.

A. Preliminaries on contact force modeling

Consider a robot coming into contact with a rigid surface. When both bodies are assumed to be perfectly rigid, no deformation can occur, and physical penetration is impossible. This implies a non-penetration condition, which can be expressed as a unilateral constraint on the geometric distance ϕ between them [22], requiring $\phi \geq 0$ to prevent interpenetration. Specifically, a complementarity relationship arises between the contact force and the distance separating the two entities: either (i) the contact force is zero and $\phi > 0$, meaning the bodies are not in contact, or (ii) the contact force is non-zero and $\phi = 0$, indicating active contact. To formally capture this interaction, we adopt the LCP framework [14], which will be introduced in Section II-B. For the readers' convenience, it is worth to notice that ϕ can, in general, be any differentiable function of the system state, as long as it is non-negative. As an example, in Section II-C.2, ϕ will denote the remaining length of a cable before it becomes taut.

B. Linear Complementarity Problem formulation

Consider a generic robot that comes into contact with a frictionless surface. In this case, the contact force is always normal to the surface and, as discussed in [23], [24], a solution to the corresponding LCP is known to always exist.

Let $\boldsymbol{q}$, $\dot{\boldsymbol{q}}$, and $\ddot{\boldsymbol{q}}$ be the generalized coordinates, velocity, and acceleration respectively, of the considered robot. Its equations of motion can be expressed as:

$$\boldsymbol{M}(\boldsymbol{q})\ddot{\boldsymbol{q}} = \boldsymbol{\tau}(\boldsymbol{q}, \dot{\boldsymbol{q}}) + \boldsymbol{B}(\boldsymbol{q})\boldsymbol{u} + \boldsymbol{J}(\boldsymbol{q})^T f^{\text{int}} \tag{1}$$

where $\boldsymbol{M}(\boldsymbol{q})$ represents the robot's inertia matrix, $\boldsymbol{\tau}(\boldsymbol{q}, \dot{\boldsymbol{q}})$ is the vector of external forces acting on the robot (e.g., gravity, Coriolis, drag etc.), $\boldsymbol{B}(\boldsymbol{q})$ is the input matrix and $\boldsymbol{u}$ is the applied control vector (e.g., thrust forces). Moreover, $\boldsymbol{J}(\boldsymbol{q})$ represents the contact Jacobian that maps the generalized coordinates to the normal contact coordinate $\boldsymbol{n}$. In particular, $\boldsymbol{J}(\boldsymbol{q}) = \partial\phi(\boldsymbol{q})/\partial\boldsymbol{q} = \nabla_{\boldsymbol{q}}^T\phi(\boldsymbol{q})$. Finally, f^{int} is the magnitude of the interaction force.

Discretizing (1) by using Euler integration with time step Δt, we derive the following discrete-time model

$$\begin{cases} \boldsymbol{q}_{k+1} = \boldsymbol{q}_k + \dot{\boldsymbol{q}}_{k+1}\Delta t \\ \dot{\boldsymbol{q}}_{k+1} = \dot{\boldsymbol{q}}_k + \boldsymbol{M}_k^{-1}\left(\boldsymbol{\tau}_k\Delta t + \boldsymbol{B}_k\boldsymbol{u}_k\Delta t + \boldsymbol{J}_k^T f_{k+1}^{\text{int}}\Delta t\right) \end{cases} \tag{2}$$

where $\boldsymbol{q}_k = \boldsymbol{q}(t_k)$, $\boldsymbol{J}_k = \boldsymbol{J}(\boldsymbol{q}_k)$, and the same notation applies to the remaining symbols.

A more compact representation of (2) can be written as

$$\begin{pmatrix} \boldsymbol{q}_{k+1} \\ \dot{\boldsymbol{q}}_{k+1} \end{pmatrix} = \boldsymbol{f}(\boldsymbol{q}_k, \boldsymbol{u}_k) = \begin{pmatrix} \boldsymbol{q}_k + \dot{\boldsymbol{q}}_{k+1}\Delta t \\ \boldsymbol{M}_k^{-1}\left(\boldsymbol{c}_k + \boldsymbol{J}_k^T f_{k+1}^{\text{int}}\Delta t\right) \end{pmatrix} \tag{3}$$

where

$$\boldsymbol{c}_k = \boldsymbol{M}_k\dot{\boldsymbol{q}}_k + \boldsymbol{\tau}_k\Delta t + \boldsymbol{B}_k\boldsymbol{u}_k\Delta t. \tag{4}$$

Denoting with

$$\lambda_{k+1} = f_{k+1}^{\text{int}}\Delta t \tag{5}$$

the interaction impulse and recalling that ϕ is a function supposed to be non-negative, we can obtain a LCP formulation by imposing the unilateral constraint $\phi(\boldsymbol{q}_{k+1}) \geq 0$. This, according to [15], can be written as

$$\begin{aligned} \phi(\boldsymbol{q}_{k+1}) &= \phi(\boldsymbol{q}_k) + \Delta t\ \boldsymbol{J}_k\dot{\boldsymbol{q}}_{k+1} \\ &= \phi(\boldsymbol{q}_k) + \Delta t\ \boldsymbol{J}_k\boldsymbol{M}_k^{-1}\left(\boldsymbol{c}_k + \boldsymbol{J}_k^T\lambda_{k+1}\right) \geq 0 \end{aligned} \tag{6}$$

and is equivalent to the compact form

$$\phi(\boldsymbol{q}_{k+1}) = a_k\lambda_{k+1} + b_k \geq 0 \tag{7}$$

where

$$\begin{aligned} a_k &= \boldsymbol{J}_k\boldsymbol{M}_k^{-1}\boldsymbol{J}_k^T\ \Delta t \\ b_k &= \phi(\boldsymbol{q}_k) + \boldsymbol{J}_k\boldsymbol{M}_k^{-1}\boldsymbol{c}_k\ \Delta t \\ &= \phi(\boldsymbol{q}_k) + \Delta t\ \boldsymbol{J}_k\left(\dot{\boldsymbol{q}}_k + \boldsymbol{M}_k^{-1}\boldsymbol{\tau}_k\Delta t + \boldsymbol{M}_k^{-1}\boldsymbol{B}_k\boldsymbol{u}_k\Delta t\right) \end{aligned}$$

An additional constraint stems from the non-adhesive nature of contact, which requires that the interaction impulse satisfies $\lambda_{k+1} \geq 0$. Moreover, as discussed in Section II-A, the interaction impulse λ_{k+1} and the distance function $\phi(\boldsymbol{q}_{k+1})$ are complementary – that is, they cannot both be strictly positive simultaneously. Together with (7), these conditions can be compactly expressed in LCP form as:

$$0 \leq \lambda_{k+1} \perp a_k\lambda_{k+1} + b_k \geq 0 \tag{8}$$

Finally, the impulse λ_{k+1}, that prevent penetration between the bodies, is computed by solving an LCP at each simulation time step. To this aim, we employed the so-called Lemke's algorithm (see, e.g., [14] for more details).

Briefly, after discretizing the system's equation of motion and starting from the assumption of no contact as initial condition, one has to compute, at every time step, the next interaction impulse λ_{k+1} from (8). λ_{k+1} – and, more specifically, the interaction force f_{k+1}^{int} derived from it via (5) – will be incorporated into the predictive model of the MPC controller, as detailed in Section III.

C. Case studies

To prove the validity of the LCP formulation in modeling different kinds of interaction forces, two case studies are considered in this paper: (i) a quadrotor coming into contact with a frictionless surface; and (ii) a quadrotor that lifts a cable-suspended payload. Both case studies are modeled using (1). Furthermore, for each case, a suitable expression for the unilateral constraint $\phi(\boldsymbol{q}_{k+1}) \geq 0$ will be derived (see Section II-C.1 and Section II-C.2), enabling the formulation of a corresponding LCP in the form (8), which allows the computation of the interaction forces that will be used within an MPC controller (see Section III).

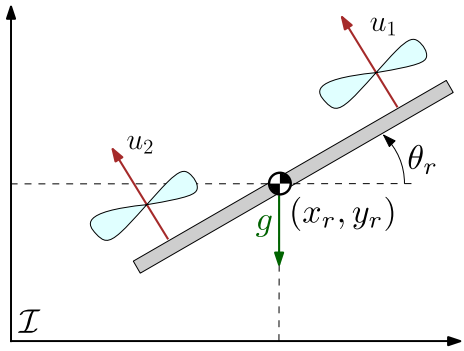

Fig. 1. The planar quadrotor considered. In particular, x_r and y_r are the CoM position of the robot, θ_r is its orientation, all expressed in an inertial reference frame $\mathcal{I}$. Moreover, u_1 and u_2 are the thrust forces of the drone's propellers and g is the gravitational acceleration.

1) Aerial robot contacting with a surface: The first physical system that we consider as a benchmark is an AAV that should land on a frictionless surface. The interaction force considered in this case is the contact force.

To simplify the problem, we assume that the quadrotor's motion is constrained to a plane, reducing the problem to a two-dimensional setting. Additionally, we assume that the quadrotor is condensed in its center of mass (CoM), so that the contact force is always applied at this point. This approximation allows us to neglect potential contacts between the propellers and the surface. Possible real systems that well suit this approximation are the encaged quadrotors, i.e., AAVs equipped with an external protective and rolling structure with a circular section, e.g., a sphere or a cylinder (see, e.g., [12] and [13]). These systems are specifically designed to interact with surfaces protecting the propellers from impact against them.

Let $\boldsymbol{q}$ be the pose of the robot, with x_r, y_r representing its center of mass position and θ_r its orientation, all expressed in an inertial reference frame $\mathcal{I}$, as shown in Fig. 1. The system model can be expressed in the form (1) by choosing:

$$\boldsymbol{q} = \begin{bmatrix} x_r & y_r & \theta_r \end{bmatrix}^T$$

$$\boldsymbol{M} = \begin{bmatrix} m_r & 0 & 0 \\ 0 & m_r & 0 \\ 0 & 0 & I_r \end{bmatrix} \quad \boldsymbol{\tau} = \begin{bmatrix} 0 \\ -m_r g \\ 0 \end{bmatrix}$$

$$\boldsymbol{B} = \begin{bmatrix} -\sin\theta_r & -\sin\theta_r \\ \cos\theta_r & \cos\theta_r \\ d_r & -d_r \end{bmatrix} \quad \boldsymbol{u} = \begin{bmatrix} u_1 \\ u_2 \end{bmatrix},$$

where m_r is the mass of the robot, I_r is its moment of inertia, and d_r is the distance between the center of mass and the base of the propellers; $\boldsymbol{u}$ is the vector of the thrust forces of the propellers of the drone; f^{int} is the magnitude of the contact force normal to the contacting surface.

In this case study, we considered $\phi(\boldsymbol{q})$ as the geometric distance between the robot CoM and the external boundary of the surface, supposed to be spherical for sake of simplicity, i.e.,

$$\phi(\boldsymbol{q}) = \sqrt{(x_r - x_s)^2 + (y_r - y_s)^2} - R_s, \tag{9}$$

where $\boldsymbol{s} = [x_s, y_s]^T$ is the center of the surface in $\mathcal{I}$ and R_s its radius.

2) Aerial robot lifting a cable-suspended payload: In this scenario, the aerial robot should lift a mass connected to the quadrotor via a cable, as in [21].

Consider a point mass suspended through a massless and unstreatchable cable from the quadrotor CoM. This system can be modeled through (1) by choosing:

$$\boldsymbol{q} = \begin{bmatrix} x_r & y_r & \theta_r & x_p & y_p \end{bmatrix}^T$$

$$\boldsymbol{M} = \begin{bmatrix} m_r & 0 & 0 & 0 & 0 \\ 0 & m_r & 0 & 0 & 0 \\ 0 & 0 & I_r & 0 & 0 \\ 0 & 0 & 0 & m_p & 0 \\ 0 & 0 & 0 & 0 & m_p \end{bmatrix} \quad \boldsymbol{\tau} = \begin{bmatrix} 0 \\ -m_r g \\ 0 \\ 0 \\ -m_p g \end{bmatrix}$$

$$\boldsymbol{B} = \begin{bmatrix} -\sin\theta_r & -\sin\theta_r \\ \cos\theta_r & \cos\theta_r \\ d_r & -d_r \\ 0 & 0 \\ 0 & 0 \end{bmatrix} \quad \boldsymbol{u} = \begin{bmatrix} u_1 \\ u_2 \end{bmatrix},$$

where $x_r, y_r, \theta_r, m_r, I_r$ are robot-related quantities defined in Section II-C.1. Moreover, $\boldsymbol{p} = [x_p, y_p]^T$ is the position of the point-mass payload with respect to $\mathcal{I}$ and m_p is the point-mass payload. Finally, f^{int} in (1) is the magnitude of the tension force acting on the cable between the point mass payload and the quadrotor.

This scenario is completely different from the previous one: here there are no contact forces and surfaces to interact with. Anyway, we could apply the same theory about interaction force modeling and the related LCP: specifically, one can take into account as interaction force the tension force of the cable when it is taut (instead of the contact force) and as function ϕ the expression

$$\phi(\boldsymbol{q}) = L_p - \sqrt{(x_r - x_p)^2 + (y_r - y_p)^2}, \tag{10}$$

where L_p is the length of the cable when it is taut, and the second term in (10) represents the distance between the robot and the payload. The cable constrains the latter to never be greater than L_p, so that we always have $\phi(\boldsymbol{q}) \geq 0$. As for the previous case study, a complementarity condition can be formulated: when the cable is slack, the tension force f^{int} is zero and ϕ is positive; conversely, when the cable is taut, a non-zero tension force f^{int} arises and ϕ becomes zero.

III. The Proposed MPC

This section describes how to integrate the LCP formulation described in Section II-B within an MPC framework. Given the dynamic model in (3) and defining the system state at a generic time instant t_k as $\boldsymbol{x}_k = \boldsymbol{x}(t_k) = \begin{bmatrix} \boldsymbol{q}_k^T & \dot{\boldsymbol{q}}_k^T \end{bmatrix}^T$, our MPC iteratively solves the following optimal control problem

$$\min_{(\boldsymbol{X}, \boldsymbol{U})} \quad J(\boldsymbol{X}, \boldsymbol{U}) \tag{11a}$$

$$\text{s.t.} \quad \boldsymbol{x}(t_k) = \boldsymbol{x}_0, \tag{11b}$$

$$\boldsymbol{x}_{k+1} = \boldsymbol{f}(\boldsymbol{x}_k, \boldsymbol{u}_k) \tag{11c}$$

where $\boldsymbol{u}_k$ is the control input of the system at generic time instant t_k, $\boldsymbol{x}_0$ is the current state of the system, and $\boldsymbol{X} = \{\boldsymbol{x}_0, \dots, \boldsymbol{x}_N\}$, $\boldsymbol{U} = \{\boldsymbol{u}_0, \dots, \boldsymbol{u}_{N-1}\}$. In addition, $\boldsymbol{f}$ in (11c) – whose expression is in (3) – is the dynamic function that describes the state evolution from $\boldsymbol{x}_k$ to $\boldsymbol{x}_{k+1}$ given the control $\boldsymbol{u}_k$.

The cost function J in (11a) to minimize is defined as

$$J(\boldsymbol{X}, \boldsymbol{U}) = \sum_{k=0}^{N-1} l(\boldsymbol{x}_k, \boldsymbol{u}_k) + l_f(\boldsymbol{x}_N) \tag{12}$$

where $l(\boldsymbol{x}_k, \boldsymbol{u}_k)$ is the running cost, $l_f(\boldsymbol{x}_N)$ is the terminal cost term and N is the considered horizon length. Specifically, these functions are chosen to be quadratic in order to employ the iLQR algorithm, that is

$$l(\boldsymbol{x}_k, \boldsymbol{u}_k) = (\boldsymbol{x}_k - \boldsymbol{x}_g)^T \boldsymbol{Q} (\boldsymbol{x}_k - \boldsymbol{x}_g) + \boldsymbol{u}_k^T \boldsymbol{R} \boldsymbol{u}_k \tag{13}$$

$$l_f(\boldsymbol{x}_N) = (\boldsymbol{x}_N - \boldsymbol{x}_g)^T \boldsymbol{Q}_T (\boldsymbol{x}_N - \boldsymbol{x}_g) \tag{14}$$

It is important to note that the optimal control problem defined in (11a–11b–11c) explicitly depends on the LCP condition described in (8). Specifically, for a robot whose dynamics is given by (3), the function $\boldsymbol{f}$ corresponds to the right-hand side of that equation. Since this expression explicitly depends on the interaction force f_{k+1}^{int}, the predictive model (11c) used in the MPC formulation inherently depends on f_{k+1}^{int} as well. Consequently, computing f_{k+1}^{int} is necessary to solve the MPC problem. To this end, we employ the methodology presented in Section II-B: using Lemke's algorithm, the interaction impulse λ_{k+1} is first obtained from the LCP in (8), and the corresponding interaction force f_{k+1}^{int} is then computed via (5). In other words, we have two nested optimization problems to be solved: (i) an inner one, that is in charge of computing f_{k+1}^{int} by first solving the LCP in (8) and then applying (5); and (ii) an outer one, i.e., (11a-11b-11c), solved by the MPC that uses f_{k+1}^{int} in (11c).

Following the receding horizon principle, the optimal control problem (11a–11b–11c) is iteratively solved at each time instant to obtain the control sequence $\boldsymbol{U}$, of which only the first input $\boldsymbol{u}_0$ is applied to the system. The optimization is then repeated at the next sampling instant.

IV. Simulations and Results

In this section, simulation results that validate the proposed approach are reported. In both case studies, we start from the assumption of zero interaction force as an initial condition. It well suits the two examined case studies: for the first, it implies an initial position of the aerial robot that is far from the surface, and for the second it reflects the initial slack condition of the cable connecting the robot and the payload[1].

The two scenarios highlight the capability of our framework to handle distinct complementarity conditions and demonstrate a key advantage of embedding the LCP formulation within an MPC controller: it enables a unified model within the MPC formulation, without the need to manually divide the task into separate phases or implement switching strategies, as would be required if different models were used across different task stages (see, e.g., [21]).

[1]A video illustrating the different simulation scenarios is available at: `https://www.laas.fr/en/homepages/rfuser/research/linear-complementarity-mpc/`.

TABLE I

Simulation parameters for the scenario where a quadrotor has to reach a desired goal state $\boldsymbol{x}_g$ on a rigid surface. The MPC state for this scenario is: $\boldsymbol{x} = [x_r, y_r, \theta_r, \dot{x}_r, \dot{y}_r, \dot{\theta}_r]^T$.

Quadrotor	
m_r	$1\,\text{kg}$
I_r	$11.7 \cdot 10^{-3}\,\text{kg} \cdot \text{m}^2$
d_r	$0.1\,\text{m}$
Simulation	
Δt	$0.01\,\text{s}$
N	100
Surface	
x_s	$1\,\text{m}$
y_s	$0.85\,\text{m}$
R_s	$0.15\,\text{m}$
Cost function J	
$\boldsymbol{Q}$	$\text{diag}(100, 100, 0, 10, 10, 1)$
$\boldsymbol{R}$	$\text{diag}(1, 1)$
$\boldsymbol{Q_T}$	$\text{diag}(1000, 1000, 1000, 1, 1, 1)$
Initial State $\boldsymbol{x}_0$	
Quadrotor	$x_{r,0} = 0.9\,\text{m}$, $y_{r,0} = 1.1\,\text{m}$, $\theta_{r,0} = 0.0\,\text{rad}$ $\dot{x}_{r,0} = 0.0\,\text{m/s}$, $\dot{y}_{r,0} = 0.0\,\text{m/s}$, $\dot{\theta}_{r,0} = 0.0\,\text{rad/s}$
Final Desired State $\boldsymbol{x}_g$	
Quadrotor	$x_{r,g} = 1.0\,\text{m}$, $y_{r,g} = 1.0\,\text{m}$, $\theta_{r,g} = 0.0\,\text{rad}$ $\dot{x}_{r,g} = 0.0\,\text{m/s}$, $\dot{y}_{r,g} = 0.0\,\text{m/s}$, $\dot{\theta}_{r,g} = 0.0\,\text{rad/s}$

A. Case study 1: Quadrotor interacting with a rigid surface

Consider a quadrotor that is tasked with reaching a desired state – denoted with $\boldsymbol{x}_g$ – placed on a frictionless surface. This surface is modeled as a sphere, whose center and radius are assumed to be known. These geometric quantities are used for computing the unilateral constraint of this case study, where $\phi(\boldsymbol{q})$ is the geometric distance between the quadrotor center of mass and the surface.

The parameters used for this application scenario are reported in Tab. I. We performed several simulations, depicting two resulting trajectories in Fig. 2. These trajectories differ for the value assigned to $\boldsymbol{R}$ in (13), being $\boldsymbol{R} = 0.01\ \boldsymbol{I}_2$ in the first case and $\boldsymbol{R} = \boldsymbol{I}_2$ in the second one, where $\boldsymbol{I}_2$ is the 2×2 identity matrix. In the former case, $\boldsymbol{R}$ is chosen in such a way the energy term in (13) is numerically smaller with respect to the state-related one. This results in a trajectory (orange line in Fig. 2) where the drone moves, in a greedy manner, to the desired state, at the price of a poor energy-efficient trajectory. On the other hand, when $\boldsymbol{R}$ is set to higher values (as for the blue trajectory in Fig. 2), the drone takes advantage of the presence of the surface, preferring to slide over it to reach the goal state in a more energy efficient way. This behavior is also confirmed by the thrust and distance plots in Fig. 2.

Finally, the contact force is reported in Fig. 2. As it can be seen from the figure, there is a spike in the contact force due to the robot that comes into contact with the surface. Notably, this abrupt behavior is not reflected in the thrust profiles, which remain relatively smooth despite the occurrence of

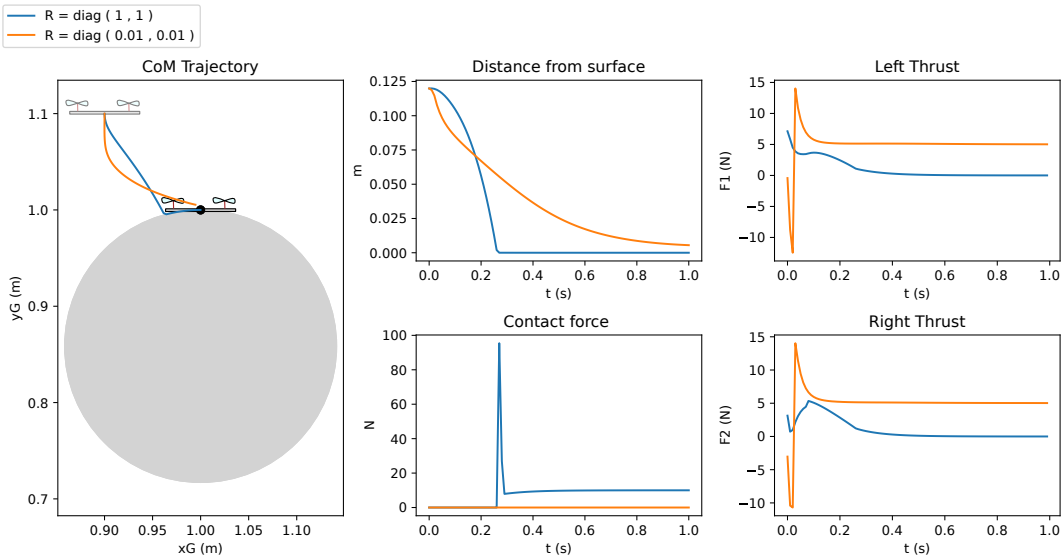

Fig. 2. Simulation results for the quadrotor tasked with reaching a desired goal state $\boldsymbol{x}_g$ on a frictionless surface. In particular, the $x-y$ robot trajectory is depicted, where the initial robot position is represented in transparency while its final configuration in solid. Furthermore, the distance to the surface, the contact force, and the left/right thrusts (inputs u_1 and u_2, respectively) of the drone are shown. Two distinct cases are shown: the blue one favors the energy term in (13) while the orange one priorities the minimization of the position error, resulting in a greedier trajectory toward the goal.

contact. This can be reasonably attributed to the predictive nature of the MPC controller, which anticipates the impact moment and adjusts the thrust accordingly, resulting in smoother control inputs.

B. Case study 2: quadrotor interacting with a cable-suspended payload

In the second scenario, the quadrotor should lift a payload that is connected to the drone through an unstreatchable and massless cable. The parameters are shown in Table II and the simulation results are reported in Fig. 3.

Initially, the payload lies on the ground (black rectangle in Fig. 3) and the cable is slack (the initial configuration is in transparency in Fig. 3 with the cable in purple). The goal is to move the payload from its initial position to a desired location (represented with a black dot in the figure). For doing that, the drone should lift the payload making the cable taut. Fig. 3 reports the evolution of the propellers' thrust, the remaining slack length of the cable, and the resulting tension force. As shown, the drone increases its altitude until the cable becomes taut at approximately 0.3 s, marked by a sharp increase in the tension force, thereby lifting the payload and reaching the desired state.

V. Conclusions

In this work, we proposed a modeling approach – based on the linear complementarity formulation – for aerial vehicles where an interaction force occurs. We then designed an MPC framework to perform online optimization of the aerial robot trajectory, solving the finite horizon optimal control problem using the iLQR method. We validated our approach for two case studies: (i) a quadrotor that should land on a surface, requiring to make contact with it; and (ii) a quadrotor that should lift a cable-suspanded payload, switching from a slack to a taut cable conditions. The simulations confirmed the validity of our approach. Future work will focus on extending the proposed framework to account for frictional surfaces by considering the tangential components of the contact

TABLE II

Simulation parameters for the scenario where a quadrotor must lift a cable-suspended payload up to a desired state $\boldsymbol{x}_g$. The MPC state is: $\boldsymbol{x} = [x_r, y_r, \theta_r, x_p, y_p, \dot{x}_r, \dot{y}_r, \dot{\theta}_r, \dot{x}_p, \dot{y}_p]^T$.

Quadrotor	
m_r	$1\,\text{kg}$
I_r	$11.7 \cdot 10^{-3}\,\text{kg} \cdot \text{m}^2$
d_r	$0.1\,\text{m}$
Payload	
m_p	$0.1\,\text{kg}$
Cable	
L_p	$1\,\text{m}$
Simulation	
Δt	$0.01\,\text{s}$
N	100
Cost function J	
$\boldsymbol{Q}$	$\text{diag}(100, 100, 10, 1000, 100, 1, 1, 1, 1, 1)$
$\boldsymbol{R}$	$\text{diag}(0.1, 0.1)$
$\boldsymbol{Q}_T$	$\text{diag}(1000, 1000, 100, 1000, 1000, 1, 1, 1, 1, 1)$
Initial State $\boldsymbol{x}_0$	
Quadrotor	$x_{r,0} = -0.2\,\text{m}$, $y_{r,0} = 0.4\,\text{m}$, $\theta_{r,0} = 0.0\,\text{rad}$ $\dot{x}_{r,0} = 0.0\,\text{m/s}$, $\dot{y}_{r,0} = 0.0\,\text{m/s}$, $\dot{\theta}_{r,0} = 0.0\,\text{rad/s}$
Payload	$x_{p,0} = 0.0\,\text{m}$, $y_{p,0} = 0.0\,\text{m}$ $\dot{x}_{p,0} = 0.0\,\text{m/s}$, $\dot{y}_{p,0} = 0.0\,\text{m/s}$
Final Desired State $\boldsymbol{x}_g$	
Quadrotor	$x_{r,g} = 0.0\,\text{m}$, $y_{r,g} = 1.2\,\text{m}$, $\theta_{r,g} = 0.0\,\text{rad}$ $\dot{x}_{r,g} = 0.0\,\text{m/s}$, $\dot{y}_{r,g} = 0.0\,\text{m/s}$, $\dot{\theta}_{r,g} = 0.0\,\text{rad/s}$
Payload	$x_{p,g} = 0.0\,\text{m}$, $y_{p,g} = 0.2\,\text{m}$ $\dot{x}_{p,g} = 0.0\,\text{m/s}$, $\dot{y}_{p,g} = 0.0\,\text{m/s}$

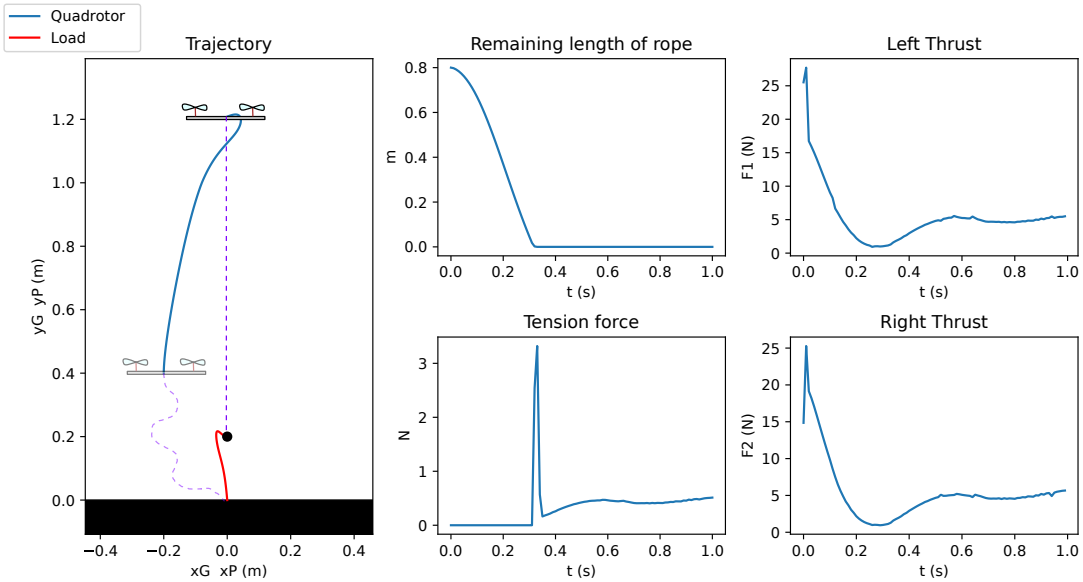

Fig. 3. Simulation results for the quadrotor tasked with lifting a cable-suspended mass up to a desired goal state. In particular, the $x-y$ robot and mass trajectories are depicted, where the purple line represents the cable and the initial configuration of the system is represented in transparency. Furthermore, the tension force, and the remaining length of the cable before it becomes taut are shown, together with the left/right thrusts (inputs) of the drone.

force. Additionally, the formulation will be expanded to include flexible or deformable cables. Finally, the proposed methodology will be experimentally validated on real drones.

REFERENCES

[1] A. Ollero, M. Tognon, A. Suarez, D. Lee, and A. Franchi, "Past, present, and future of aerial robotic manipulators," *IEEE Transactions on Robotics*, vol. 38, no. 1, pp. 626–645, 2021.

[2] A. Srour, S. Marcellini, T. Belvedere, M. Cognetti, A. Franchi, and P. Robuffo Giordano, "Experimental validation of sensitivity-aware trajectory planning for a quadrotor uav under parametric uncertainty," in *2024 Int. Conf. on Unmanned Aircraft Systems*, pp. 572–578, 2024.

[3] A. Alcántara, J. Capitán, A. Torres-González, R. Cunha, and A. Ollero, "Autonomous execution of cinematographic shots with multiple drones," *IEEE Access*, vol. 8, pp. 201300–201316, 2020.

[4] P. Petráček, V. Krátkỳ, and M. Saska, "Dronument: System for reliable deployment of micro aerial vehicles in dark areas of large historical monuments," *IEEE Robotics and Automation Letters*, vol. 5, no. 2, pp. 2078–2085, 2020.

[5] M. Selvaggio, M. Cognetti, S. Nikolaidis, S. Ivaldi, and B. Siciliano, "Autonomy in physical human-robot interaction: A brief survey," *IEEE Robotics and Automation Letters*, vol. 6, no. 4, pp. 7989–7996, 2021.

[6] M. A. Trujillo, J. R. Martínez-de Dios, C. Martín, A. Viguria, and A. Ollero, "Novel aerial manipulator for accurate and robust industrial ndt contact inspection: A new tool for the oil and gas inspection industry," *Sensors*, vol. 19, no. 6, p. 1305, 2019.

[7] A. Ollero, G. Heredia, A. Franchi, G. Antonelli, K. Kondak, A. Sanfeliu, A. Viguria, J. R. Martinez-de Dios, F. Pierri, J. Cortés, *et al.*, "The aeroarms project: Aerial robots with advanced manipulation capabilities for inspection and maintenance," *IEEE Robotics & Automation Magazine*, vol. 25, no. 4, pp. 12–23, 2018.

[8] N. Nikhil, S. Shreyas, G. Vyshnavi, and S. Yadav, "Unmanned aerial vehicles (uav) in disaster management applications," in *2020 Third Int. Conf. on Smart Systems and Inventive Technology (ICSSIT)*, pp. 140–148, IEEE, 2020.

[9] I. Palunko, P. Cruz, and R. Fierro, "Agile load transportation: Safe and efficient load manipulation with aerial robots," *IEEE robotics & automation magazine*, vol. 19, no. 3, pp. 69–79, 2012.

[10] M. Tognon, C. Gabellieri, L. Pallottino, and A. Franchi, "Aerial co-manipulation with cables: The role of internal force for equilibria, stability, and passivity," *IEEE Robotics and Automation Letters*, vol. 3, no. 3, pp. 2577–2583, 2018.

[11] C. Gabellieri, M. Tognon, D. Sanalitro, and A. Franchi, "Force-based pose regulation of a cable-suspended load using uavs with force bias," in *2023 IEEE/RSJ Int. Conf. on Intelligent Robots and Systems (IROS)*, pp. 6920–6926, IEEE, 2023.

[12] A. Briod, P. Kornatowski, J.-C. Zufferey, and D. Floreano, "A collision-resilient flying robot," *Journal of Field Robotics*, vol. 31, no. 4, pp. 496–509, 2014.

[13] A. Kalantari and M. Spenko, "Design and experimental validation of hytaq, a hybrid terrestrial and aerial quadrotor," in *2013 IEEE Int. Conf. on Robotics and Automation*, pp. 4445–4450, IEEE, 2013.

[14] R. W. Cottle, J.-S. Pang, and R. E. Stone, *The linear complementarity problem*. SIAM, 2009.

[15] Y. Tassa, T. Erez, and E. Todorov, "Synthesis and stabilization of complex behaviors through online trajectory optimization," in *2012 IEEE/RSJ Int. Conf. on Intelligent Robots and Systems*, pp. 4906–4913, IEEE, 2012.

[16] J. Rawlings, D. Mayne, and M. Diehl, *Model Predictive Control: Theory, Computation, and Design*. Nob Hill Publishing, 2017.

[17] D. Mayne, J. Rawlings, C. Rao, and P. Scokaert, "Constrained model predictive control: Stability and optimality," *Automatica*, vol. 36, no. 6, pp. 789–814, 2000.

[18] T. Belvedere, M. Cognetti, G. Oriolo, and P. Robuffo Giordano, "Sensitivity-aware model predictive control for robots with parametric uncertainty," *IEEE Transactions on Robotics*, pp. 1–20, 2025.

[19] W. Li and E. Todorov, "Iterative linear quadratic regulator design for nonlinear biological movement systems," in *Proceedings of the First Int. Conf. on Informatics in Control, Automation and Robotics - Volume 1: ICINCO,*, pp. 222–229, INSTICC, SciTePress, 2004.

[20] E. Todorov and W. Li, "A generalized iterative lqg method for locally-optimal feedback control of constrained nonlinear stochastic systems," in *Proceedings of the 2005, American Control Conference, 2005.*, pp. 300–306 vol. 1, 2005.

[21] P. J. Cruz and R. Fierro, "Cable-suspended load lifting by a quadrotor uav: hybrid model, trajectory generation, and control," *Autonomous Robots*, vol. 41, pp. 1629–1643, 2017.

[22] P. Flores, "Contact mechanics for dynamical systems: a comprehensive review," *Multibody System Dynamics*, pp. 1–51, 2022.

[23] M. Anitescu and F. A. Potra, "Formulating dynamic multi-rigid-body contact problems with friction as solvable linear complementarity problems," *Nonlinear Dynamics*, vol. 14, pp. 231–247, 1997.

[24] P. Lötstedt, "Mechanical systems of rigid bodies subject to unilateral constraints," *SIAM Journal on Applied Mathematics*, vol. 42, no. 2, pp. 281–296, 1982.